IEEE Access
Multidisciplinary | Rapid Review | Open Access Journal

Received May 4, 2020, accepted May 21, 2020, date of publication May 26, 2020, date of current version June 5, 2020.

Digital Object Identifier 10.1109/ACCESS.2020.2997865

Design of Smart Brain Oxygenation Monitoring System for Estimating Cardiovascular Disease Severity

WILLY CHOU[1], PEI-JUNG WU[2], CHIH-CHIEH FANG[3], YUN-SHAN YEN[4], AND BOR-SHYH LIN[3,5], (Senior Member, IEEE)

[1]Department of Rehabilitation, Chi Mei Medical Center, Tainan 71004, Taiwan
[2]College of Information and Distribution Science, National Taichung University of Science and Technology, Taichung 40401, Taiwan
[3]Institute of Imaging and Biomedical Photonics, National Chiao Tung University, Tainan 71150, Taiwan
[4]Division of Rehabilitation Medicine, Ditmanson Medical Foundation Chia-Yi Christian Hospital, Chiayi 600566, Taiwan
[5]Department of Medical Research, Chi Mei Medical Center, Tainan 71004, Taiwan

Corresponding author: Bor-Shyh Lin (borshyhlin@gmai.com)

This work was supported in part by the Ministry of Science and Technology, Taiwan, under Grant MOST 108-2221-E-009-054-MY2, in part by the Higher Education Sprout Project of National Chiao Tung University and Ministry of Education (MOE), Taiwan, and in part by the Chi Mei Medical Center, Taiwan.

ABSTRACT Clinically, cardiovascular disease (CVD) patients need physicians to suggest different exercise training and rehabilitation procedures to improve their cardiopulmonary function (CPF). In previous studies, several approaches, such as cardiopulmonary exercise testing (CPET), echocardiography and computed tomography angiography (CTA), were proposed to indirectly estimate the rehabilitation effect on CPF. However, the above approached require experienced operators and complex equipment. In this study, a smart and wearable brain oxygenation monitoring system without motion artifact and crosstalk is proposed to estimate the blood circulation state of brain tissue directly during incremental exercise. Moreover, the technique of neural network is also used for classifying different CPF groups from the indexes extracted from the measured hemoglobin parameters. The experimental results show that the defined indexes extracted from the hemoglobin parameters can present the state of CPF, and the proposed smart brain oxygenation monitoring system can also effectively and automatically classify different CPF groups from these indexes via artificial intelligence. The proposed system therefore may assist physicians in the clinical evaluation of the CVD severity and rehabilitation effect on CPF in the future.

INDEX TERMS Brain oxygenation, cardiovascular diseases, cardiopulmonary exercise testing, neural network.

I. INTRODUCTION

Cardiovascular diseases (CVD), including cerebrovascular disease, heart diseases and vascular diseases, are one of top ten causes of death globally. World health organization (WHO) estimated that approximate 17.3 million people died from CVD per year, and the expected number of people died from CVD might increase to over 23.6 million by 2030 [1]. The previous study indicated that one of current methods of CVD prevention and treatment was exercise training and rehabilitation, which could reduce the morbidity of cardiovascular (CV) events and improve the athletic ability, quality of life and life expectancy of patients [2]. However, patients with different CVD severities require different prescriptions of training and rehabilitation programs. For this reason, how to estimate the CVD severity of the patients is useful for the treatment procedure.

In clinical practice, several approaches are used for estimating the CV function of the patients, including cardiopulmonary exercise testing (CPET), echocardiography, and computed tomography angiography (CTA). CPET is a clinical test by exercise that measures the heart ability in a controlled clinical condition and provides valuable diagnostic and prognostic information for patients with CV and pulmonary disease by using various parameters, such as oxygen uptake (V_{O_2}), carbon dioxide output (V_{CO_2}) and ventilation (V_E) of gas exchange, electrocardiogram (ECG) findings and symptoms [3]. However, the above method contains some

The associate editor coordinating the review of this manuscript and approving it for publication was Yue Zhang.

disadvantages, including the inconvenience of using the gas mask to measure gas parameters, and the influence of ECG electrode sliding caused by sweat during exercise. Echocardiography is a noninvasive imaging technique used for detecting cardiac structures and cardiac function assessment via ultrasound reflection, and calculates cardiac blood flow and tissue velocities through Doppler equation to provide a cardiac diagnosis of the patients [4]. However, this method requires more expensive cost and professional clinical staff to operate. Moreover, tissue Doppler imaging is angle dependent. If the angle of interrogation exceeds 20 degrees, the tissue velocity may be underestimated [5]. CTA is a noninvasive angiography technique for coronary arteries that assesses obstructive coronary artery diseases (CAD) via electron beam tomography. CTA results will be classified as significant CAD (50% luminal narrowing), mild CAD (<50% stenosis) and normal coronary arteries. However, asymptomatic patients are generally not suggested to do screening test via CTA due to its significant radiation and contrast administration [6].

Near infrared spectroscopy (NIRS) is a noninvasive technique used for estimating the change of human tissue components, such as the hemoglobin concentrations, and has been widely applied in many biomedical applications [7]. In 2009, Waxman *et al.* proposed a novel catheter-based NIRS system to detect lipid core coronary plaques in the coronary [8]. In 2012, Rao *et al.* used NIRS to monitor blood oxygen parameters of patients during CPET to predict the anaerobic threshold (AT) obtained by CPET [9]. The previous study also indicated that NIRS could provide non-invasive continuous assessment of the regional circulations of the venous side, and approximate global measurement and organ-specific to help the detection of circulatory abnormalities [10]. The technique of NIRS might contain the potential of estimating the CVD severity via real-time monitoring the state of blood circulation in the brain tissue. Based on the technique of NIRS, a smart brain oxygenation monitoring system for estimating cardiovascular disease severity of CVD patients is proposed in this study. Here, the cardiovascular disease severity is classified according to the peak metabolic equivalents (METs) of patients under CPET [11], [12].

In this system, a wearable optical headband is designed to non-invasively assess the blood circulation state of brain tissue during incremental exercise. From the changes of blood circulation and the peak METs, several meaningful indexes are defined and obtained to estimate the severity of CVD patient indirectly. Moreover, the technique of radial basis function neural network (RBFNN) is used for classifying patients with different CVD severity. Here, the cardiopulmonary function (CPF) estimated from CPET is used for defining the groups of different CVD severity. From the experimental results, it shows the defined parameters are significantly related to the CPF state and this proposed system can also evaluate the CPF state automatically during incremental exercise from these indexes via artificial intelligence. In the blind test stage, it shows the proposed system can provide a good performance on classification of different groups. Therefore, it may be a novel and simple method to classify different CPF groups automatically in the clinical literature.

II. METHODS AND MATERIALS

A. DESIGN OF SMART BRAIN OXYGENATION MONITORING SYSTEM

The hardware architecture of the proposed smart brain oxygenation monitoring system is shown in Fig. 1(a). It contains two parts, including a wearable optical headband and a smart platform. Here, the wearable optical headband consists of a pair of optical probes, a wireless optical signal acquisition module, and a mechanical design of headband, as shown in Fig. 1(b).

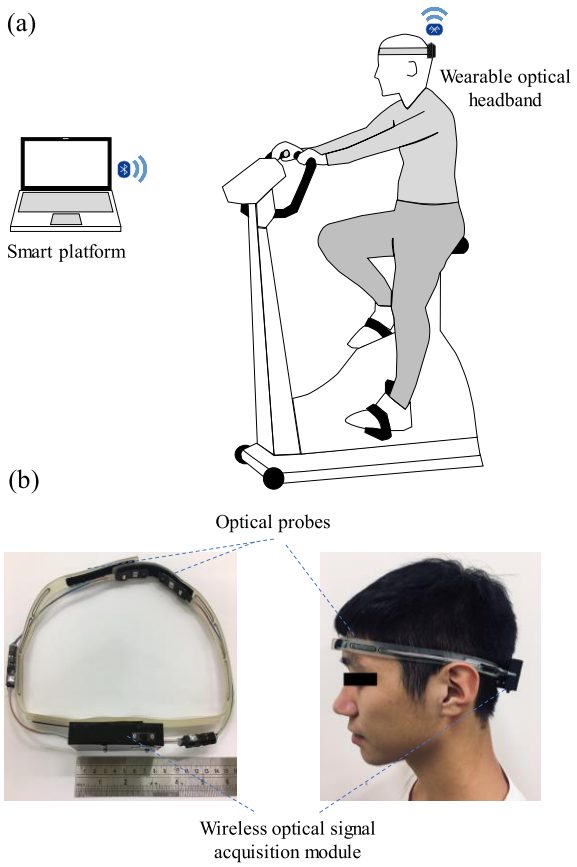

FIGURE 1. (a) Hardware architecture of proposed smart brain oxygenation monitoring system, and (b) photograph of wearable optical headband.

These optical probes contain multi-wavelengths light emitting diodes and photodiodes to provide a light source to transmit the near-infrared light into the brain tissue and receives penetrating light respectively. When the incident light transmits through the medium, the medium will cause the light attenuation due to light absorption and scattering. In this case, the relative concentrations of multiple absorbers may be estimated from the intensity change of penetrating light, caused by absorption and scattering, via the modified Beer-Lambert law (MBLL) [13], [14]. The change of the absorber

concentration will cause the optical density change of the penetrating light. The change of the optical intensity $\Delta OD(\lambda)$ caused from the change of absorber can then be expressed by

$$\Delta OD(\lambda) = -\log \frac{I_o(\lambda)}{I_i(\lambda)} = \varepsilon^{\lambda} \cdot \Delta C \cdot L \cdot B(\lambda) \quad (1)$$

where $I_o(\lambda)$ and $I_i(\lambda)$ denote the intensity of the penetrating and incident light corresponding to wavelength λ respectively, ε^{λ} is the molar extinction coefficient corresponding to wavelength λ [15], ΔC denotes the change of molar concentration of the absorber in medium, and L is the distance between the light source and the light detector. The parameter $B(\lambda)$ is the pathlength factor corresponding to wavelength λ [16]–[19], which is a correction factor used for correcting L. Consequently, $L \cdot B(\lambda)$ can be viewed as the real light path in the medium. Here, both oxyhemoglobin (HbO_2) and deoxyhemoglobin (Hb) are main absorbers in human tissues in the wavelength range of near-infrared light [18], and (1) can be simplified as followings

$$\Delta OD(\lambda) = (\varepsilon^{\lambda}_{HbO_2} \cdot \Delta[HbO_2] + \varepsilon^{\lambda}_{Hb} \cdot \Delta[Hb]) \cdot L \cdot B(\lambda) \quad (2)$$

where $\Delta[HbO_2]$ and $\Delta[Hb]$ denote the change of molar concentration of HbO_2 and Hb respectively. According to the difference between the absorption spectra of HbO_2 and Hb in the medium, dual or more wavelength light can be used for estimating $\Delta[HbO_2]$ and $\Delta[Hb]$ [13], [14]. Finally the change of molar concentration of the total hemoglobin (ΔHbT) and tissue oxygen saturation (StO_2) can be obtained from $\Delta[HbO_2]$ and $\Delta[Hb]$.

$$\Delta[HbT] = \Delta[HbO_2] + \Delta[Hb] \quad (3)$$

$$StO_2 = \frac{\Delta[HbO_2]}{\Delta[HbT]} \times 100\% \quad (4)$$

In this proposed system, the 735 nm and 850 nm wavelengths [13], [20], that straddle the isosbestic point being the superposition of the absorption spectra of HbO_2 and Hb, are used in the proposed system.

In consideration of motion artifact and crosstalk between the probes [21]–[23], a time multiplexing is implemented in order to avoid crosstalk between the probes. Moreover, these optical probes are fixed on an adjustable and flexible rubber headband. By using the flexibility of the rubber headband, these optical probes can effectively maintain a good contacting condition between the optical probes and the head to reduce the influence of motion artifact.

The block diagram of the wireless optical signal acquisition module is shown in Fig. 2. It contains a wireless transmission circuit, a microprocessor, a LED driving circuit and a PD amplification circuit. The LED drive circuit is designed to drive LEDs by the control of the microprocessor to provide multi-wavelength light. The received light signal is then converted into a voltage signal by the PD and amplified by the PD amplifying circuit. The optical signal is then digitized by an analog-to-digital converter built in the microprocessor with the sampling rate of 200 Hz. Finally, the data of the optical signal are sent to the wireless transmission circuit

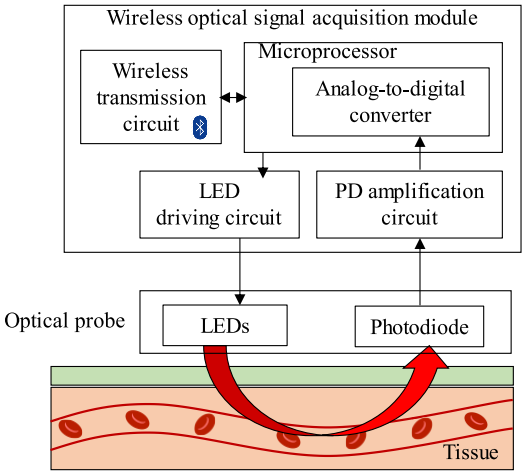

FIGURE 2. Block diagram of wireless optical signal acquisition module.

to transmit to the smart platform. After receiving these data of optical signal, the smart platform will real-time estimate the change of relative hemoglobin concentration to evaluate the physiological state of the patients. Here, the transmission through the wireless transmission circuit fits the specification of Bluetooth v4.2. The wireless optical signal acquisition module can be powered by a 3.7V 400mAh Li-ion battery.

The design of the smart platform is based on a laptop with the operational system of Windows 10. In this smart platform, a real-time monitoring application is developed by Microsoft Visual C#, to provide the basic functions of displaying analysis results and storing the raw data obtained by wearable optical headband. Three event buttons in this application are also designed to record the times and states of activity events.

B. CLASSIFICATION OF CARDIOVASCULAR DISEASE SEVERITY

In order to estimate the CVD severity, the technique of neural network is used in this study. Here, the radial basis function neural network, which is a nonlinear data modeling and contains the advantages of a faster training procedure, a better approximation capability, and a simpler network configuration, is used in this study [25], [26]. The basic structure of RBFNN contains three layers (input, hidden, and output layers), as shown in Fig 3, which contains N_0 input neurons, N_1 hidden neurons, and an output neuron. Here, standardized hemoglobin parameters are used as the input of RBFNN. Then, the output $Y(n)$ of RBFNN at n iteration can be expressed by

$$Y(n) = Z^T(n) \cdot W(n) \quad (5)$$

where $Z(n) = \left[Z_1(n), Z_2(n), \ldots, Z_{N_1}(n)\right]^T$ is the output vector of the hidden neurons, and the output $Z_k(n)$ of the k-th neuron can be calculated by the Gaussian basis function

$$Z_k(n) = \exp\left(-\frac{\|I(n) - CT_k(n)\|^2}{2\sigma^2(n)}\right) \quad (6)$$

where $I(n)$ and $\sigma(n)$ denote the vector and its standard deviation of the input neurons and $CT_k(n)$ is the center vector of the k-th hidden neuron at iteration n. The operator $\|\cdot\|$ denotes the Euclid norm between two vectors. $W(n) = [W_1(n), W_2(n), \ldots, W_{N_1}(n)]^T$ is a weight vector, and here, $W_k(n)$ is the weight between the k-th hidden neuron and the output neuron. The machine learning procedure of RBFNN contains the training and blind test stage. In the training stage, the machine learning of the center vector $CT_k(n)$ is an unsupervised learning (k-means clustering algorithm [26], [27]). The center vectors in the hidden neurons can be viewed as the prototype characteristic vectors taken from the training sets. The machine learning of the weight vector $W(n)$ is a supervised learning (normalized least mean square algorithm [26]). In the normalized least mean square algorithm, the desired signal for the better CPF group and the poorer CPF group are defined as 1 and 0, respectively. In the blind test stage, if the output of RBFNN is larger than the given threshold, it will be classified into the better CPF group; otherwise, it will be classified into the poorer CPF group.

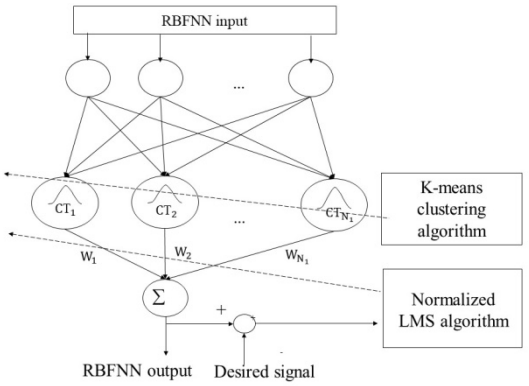

FIGURE 3. Basic structure of radial basis function neural network.

TABLE 1. Patient information corresponding to different groups.

Characteristic	Outcome	
	peak METs≧5	peak METs<5
Age (years)	51.42±11.53	57.88±10.69
Sex (Male : Female)	23:1	14:11
AMI status post PCI	12(50%)	7(28%)
CHF	7(29.17%)	4(16%)
Else diagnosis	4(16.67%)	8(32%)

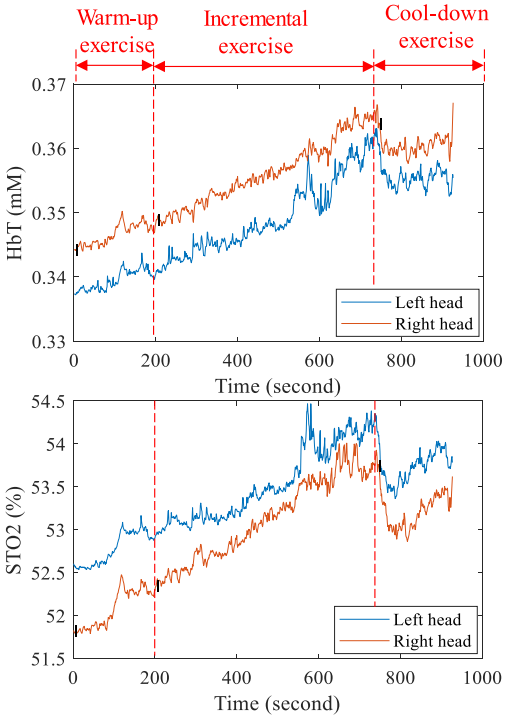

FIGURE 4. Change of hemoglobin parameters under incremental exercise.

C. EXPERIMENT DESIGN

In this study, a total of 49 adult patients attend this experiment at Chi Mei Hospital (Institutional Review Board consent number: 10602-007). Most of patients are with heart-related diseases, including acute myocardial infarction (AMI), post percutaneous coronary intervention (PCI), Congestive heart failure (CHF), etc., and the other patients are with stroke, chronic obstructive pulmonary disease (COPD), etc. The average age of the patients is 54.71 $\pm$ 11.47 years old. The information of the patients is listed in Table 1. In this experiment, the patients are instructed to wear the smart brain oxygenation monitoring system and perform CPET [3]. CPET is divided into three parts, namely warm-up exercise, incremental exercise and cool-down exercise [28]. According to their CPET results, these patients are divided into two groups of the better CPF group (peak METs 5; 23 males and 1 females) and the poorer CPF group (peak METs $<$ 5; 14 males and 11 females).

III. RESULTS

A. CHANGES OF HEMOGLOBIN PARAMETERS CORRESPONDING DIFFERENT GROUPS

The change of hemoglobin parameters (StO_2, and relative HbT concentrations) under incremental exercise are shown in Fig. 4. In this study, several indexes related to the change of hemoglobin parameters under incremental exercise are defined to describe the state of blood circulation in the brain tissue of CVD patients, and their definitions are illustrated in Fig. 5. Index I is defined as the time duration from the start to the maximum value of the hemoglobin parameter under incremental exercise. Index II is defined as the variation between the initial value and the maximum value of the hemoglobin parameter under incremental exercise. Index III is defined as the average variation of the hemoglobin parameter under incremental exercise, i.e. the sum of the hemoglobin parameter variation is divided by the time duration between the initial value and the maximum value of

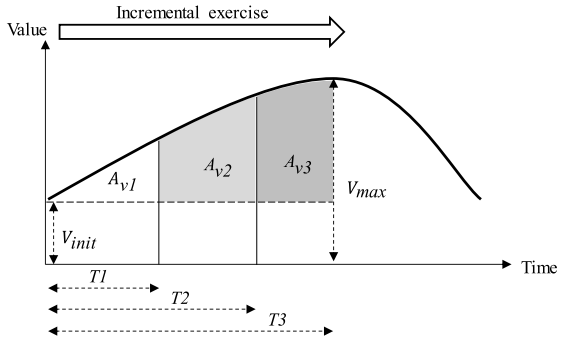

V_{init} : Initial value of hemoglobin parameter

V_{max} : Maximum value of hemoglobin parameter

A_{v1}, A_{v2}, A_{v3} : Sum of hemoglobin parameter variation

T_1 : 1 minute; T_2 : 60% of whole incremental exercise duration;

T_3 : Time duration from V_{init} to V_{max}

Index I = T_3

Index II (PII) = V_{max} - V_{init}

Index III (PIII) = $(A_{v1} + A_{v2} + A_{v3})/T_3$

Index IV (PIV) = A_{v1}/T_1

Index V = $A_{v3}/(T_3 - T_2)$

FIGURE 5. Illustration for definition of Indexes I-V related to change of hemoglobin parameters.

the hemoglobin parameter. Index IV is defined as the average variation of the hemoglobin parameter under first one-minute incremental exercise. Index V is defined as the average variation of the hemoglobin parameter between 60% of the whole incremental exercise duration and the time of the maximum hemoglobin parameter. Fig. 6(a) - Fig. 6(e) show the experimental results of Indexes I-V for different hemoglobin parameters corresponding to different groups. Except the hemoglobin parameters of Index IV for the better CPF group are lower than that of the poorer CPF group, most of Indexes I, II, II and V related to the change of StO_2, and relative HbT concentrations for the better CPF group are significantly higher than that of the poorer CPF group.

B. CLASSIFICATION PERFORMANCE OF CARDIOVASCULAR DISEASE SEVERITY

In this study, most of Indexes I, II, III and V related to the change of StO_2 and relative HbT concentration are significantly different between the better CPF group and the poorer CPF group. In this case, Indexes I, II, III and V of StO_2 and relative HbT concentrations for both of left and right foreheads are used as the input of RBFNN to classify different CPF groups. Before the classification, the optimal threshold has to be determined. Here, the threshold is set from 0 to 1 by the step of 0.1, and the numbers of the input and hidden neurons are set to 8 and 64, respectively. In order to evaluate the classification performance, several parameters for binary test have to be defined first. True-positive (TP) means better CPF is correctly identified as the better CPF group; False-positive (FP) means poorer CPF is incorrectly identified as

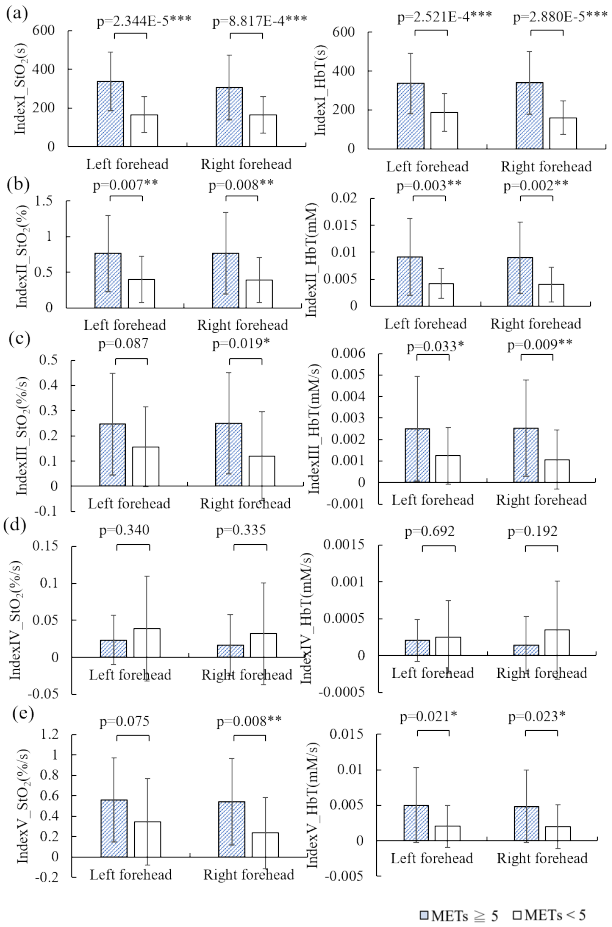

FIGURE 6. Experimental results of Indexes (a) I, (b) II, (c) III, (d) IV and (e) V related to StO2 and relative HbT corresponding to different groups. (* denotes p<0.05, ** denotes p<0.01, * denotes p<0.001).**

the better CPF group; True-negative (TN) means poorer CPF is correctly identified as the poorer CPF group; and False-negative (FN) means better CPF is incorrectly identified as the poorer CPF group. Moreover, f-measure, which is the harmonic mean of recall and precision, and accuracy are used for finding the optimal threshold and can be calculated by

$$\text{F-measure} = 2 \times \frac{precision \times recall}{precision + recall} \tag{7}$$

where $recall = \frac{TP}{TP+FN}$ is also called sensitivity, and $precision = \frac{TP}{TP+FP}$ is also called positive predictive value (PPV).

$$accuracy = \frac{TP + TN}{TP + FP + TN + FN} \tag{8}$$

In the training stage, 39 trials are used for training, and the classification performance corresponding to different thresholds are shown in Fig. 7. The optimal performance (f-measure = 79.07%, sensitivity = 70.83%, PPV = 89.47%, accuracy = 81.63%) can be obtained when the highest value of f-measure occurs and the threshold is set to 0.4 respectively. In the blind test stage, 10 trials are used, where the proposed system can provide a good performance on the classification

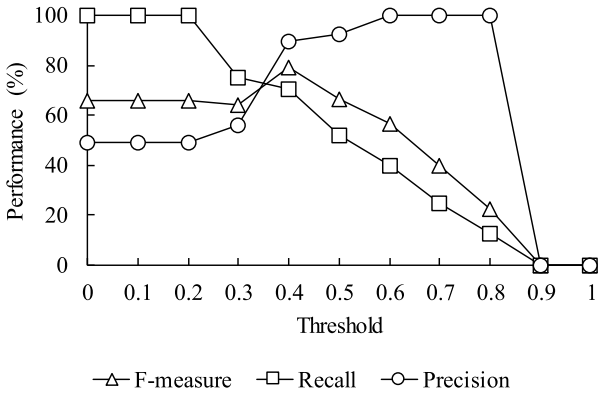

FIGURE 7. Classification performance corresponding to different thresholds in training stage.

TABLE 2. Performance of classification by using the proposed system.

		Classification by the proposed system		
		+	-	Total
Classification by the professional physician	+	3(TP)	1(FN)	4
	-	1(FP)	5(TN)	6
	Total	4	6	10

of different groups. The performance in the blind test is shown as Table 2. The accuracy, sensitivity and PPV of this proposed system are 80%, 75% and 75%, respectively. The output values of RBFNN corresponding to different groups are shown in Fig. 8. The output value of the better CPF group (0.504 ± 0.158) is significantly higher than that of the poorer CPF group (0.296 ± 0.049; p = 1.566E-4).

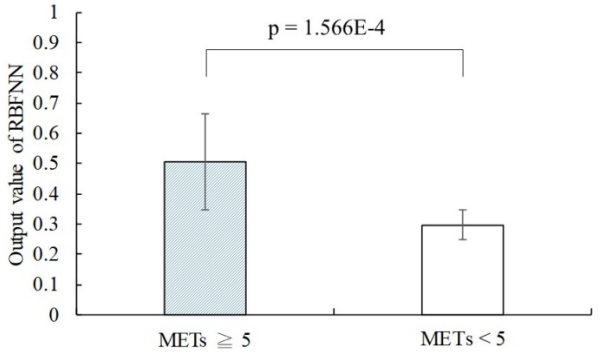

FIGURE 8. Output value of RBFNN corresponding to different group.

IV. DISCUSSION

From the experimental results in Fig. 6(a) and Fig. 6(b), Indexes I and II related to the change of StO_2 and relative HbT concentration of the better CPF group are higher than those of the poorer CPF group. These results indicate that the poorer CPF group more rapidly reaches the maximum value of these hemoglobin parameters, and the variations of these hemoglobin parameters of the poorer CPF group are less than the better CPF group. The relative HbT concentration is related to the changes in blood volume in tissue and provides an indirect indication of blood flow and perfusion [29]. This phenomenon may be explained by that the cerebral blood flow of the poorer group is relatively lower.

In 2017, Smith *et al.* collected 11 studies related to the investigation of cerebral blood flow during normoxia, acute hypoxia and chronic hypoxia, and the results showed that average relative of cerebral blood flow response was the greatest during exercise at moderate (40-70% W_{max}) intensity [30]. For this reason, the time duration between 60% of the whole incremental exercise and the time of maximum hemoglobin parameter might correspond to the intense stage of incremental exercise. From the experimental results in Fig. 6(c) and Fig. 6(e), the average variation of hemoglobin parameters of the better CPF group during the whole stage and the intense stage of incremental exercise, is higher than that of the poorer CPF group. This phenomenon of the poorer CPF group may be explained by that the cerebral circulation is relatively insufficient, especially in cardiac patients whose cardiac output fails to increase normally [31] and blood flow velocity is relatively slow. Moreover, Fig. 6(d) shows that the average variation of some hemoglobin parameters for the better CPF group is significantly lower than that of the poorer CPF group. This phenomenon may be explained by that the difference of the cerebral blood flow for different groups in the early stage of incremental exercise is unobvious.

In previous studies, several approaches were also proposed to evaluate CPF of the patients, and the comparison between the proposed system and other systems is summarized in Table 3. Here, CPET, which contains multi-sensors, including gas mask, ECG electrodes and blood pressure monitoring, to non-invasively measure V_{O_2}, V_{CO_2}, V_E, ECG, heart rate and blood pressure, can be used for evaluating CPF of the patients [3]. Before each exercise test, CPET has to be calibrated the gas exchange system by the experienced operators. Moreover, using the gas mask to measure gas parameters would easily affect the breathing activity of the user, and the ECG quality is also affected by ECG electrode sliding caused by sweat during exercise. The larger system volume, the setup of multi-sensors and the requirement of the experienced operators will cause the inconvenience of use. Echocardiography can non-invasively assess the 2D ultrasonic reflection images of cardiac structures and cardiac function via ultrasound detector, and estimates the velocity of blood flow via Doppler effect [4].

The setup is not complicated but this approach also requires the professional clinical staff to operate. Moreover, it is easily influenced by bones, and tissue Doppler imaging is angle dependent. If the angle of interrogation exceeds 20 degrees, the velocity of tissue blood flow may be underestimated [5]. CTA can be used for non-invasively assessing obstructive CAD via electron beam tomography, but the system is huge and the setup convenience is also lower. Most important of all, asymptomatic patients are not suggested to perform screening test via CTA due to its significant radiation and contrast administration [6]. Different from the above systems, the proposed system contains the advantages of small

TABLE 3. System comparison between proposed system and other systems.

	Proposed system	Cardiopulmonary exercise testing [3]	Echocardiography [4], [5]	Computed tomography angiography [6]
Sensing technique	Near-infrared spectroscopy	Gas exchange, pressure sensing	Pulsed Doppler	Angiography
Sensor type	Optic probe	Gas mask, ECG electrodes, blood pressure monitor	Ultrasound detector	Electron beam tomography
Physiological parameters	Hemoglobin parameters	V_{O_2}, V_{CO_2}, V_E,ECG, heart rate, blood pressure	Velocity of blood flow, 2-D image	2-D CTA image
Portable device	Yes	No	Yes	No
Non-invasive measurement	Yes	Yes	Yes	Yes
Transmission mode	Bluetooth	Cable	Cable	-
Setup Convenience	High	Low	Average	Low
System size	Small	Huge	Medium	Huge
Cost	Low	High	High	High
Functions	Cerebral tissue blood perfusion monitoring and automatic CPF evaluation via artificial intelligence	CPF evaluation	Cardiac structures and cardiac function assessment	Obstructive coronary artery assessment
Limitations	Limited measuring depth	Inconvenience of using gas mask; Calibrate gas exchange system; influence of ECG electrodes sliding	Influence of bones and angle dependence	Radiation; Contrast administration

size, wearability, low cost and ease of use and can access the local blood circulation state of brain tissue directly and evaluate the CPF state automatically during incremental exercise. The experimental results show that the defined parameters are significantly related to the CPF state and the proposed system can also effectively classify different CPF groups.

V. CONCLUSIONS

In this study, a smart brain oxygenation monitoring system without motion artifact and crosstalk is proposed to estimate the CVD severity of the patients. By using the technique of NIRS, the proposed system can non-invasively and real-time access the change of relative hemoglobin concentrations in the brain tissue directly. Here, because of a limited measuring depth from this proposed system, it may be slightly affected by the individual difference of brain structure. From the change of relative hemoglobin concentration under exercise, several indexes are also defined to describe the state of blood circulation in the brain tissue. From the experimental results, most of Indexes I, II, III and V related to the change of hemoglobin parameters (StO_2 and relative HbT concentration) for the better CPF group are significantly different from that of the poorer CPF group. Moreover, the CPF state can be evaluated automatically during incremental exercise from the defined indexes via artificial intelligence. In the future, the proposed system may contain the potential of assisting the physicians in the clinical evaluation of CVD severity and rehabilitation effect on CPF. Moreover, the proposed system may provide more information of rehabilitation effect on brain activation besides clinical observation in other rehabilitation applications.

REFERENCES

[1] L. J. Laslett, P. Alagona, B. A. Clark, J. P. Drozda, F. Saldivar, S. R. Wilson, C. Poe, and M. Hart, "The worldwide environment of cardiovascular disease: Prevalence, diagnosis, therapy, and policy issues," *J. Amer. College Cardiol.*, vol. 60, no. 25, pp. S1–S49, Dec. 2012.

[2] D. Hansen *et al.*, "The European association of preventive cardiology exercise prescription in everyday practice and rehabilitative training (EXPERT) tool: A digital training and decision support system for optimized exercise prescription in cardiovascular disease. Concept, definitions and construction methodology," *Eur. J. Preventive Cardiology*, vol. 24, no. 10, pp. 1017–1031, Jul. 2017.

[3] G. J. Balady, R. Arena, K. Sietsema, J. Myers, L. Coke, G. F. Fletcher, D. Forman, B. Franklin, M. Guazzi, and M. Gulati, "Clinician's guide to cardiopulmonary exercise testing in adults: A scientific statement from the American heart association," *Circulation*, vol. 122, no. 2, pp. 191–219, 2010.

[4] J. M. Gardin, "Pulsed Doppler echocardiography: An historical perspective," *J. Amer. Soc. Echocardiography*, vol. 31, no. 12, pp. 1330–1343, Dec. 2018.

[5] K. K. Kadappu and L. Thomas, "Tissue Doppler imaging in echocardiography: Value and limitations," *Heart, Lung Circulat.*, vol. 24, no. 3, pp. 224–233, Mar. 2015.

[6] M. P. Ostrom, A. Gopal, N. Ahmadi, K. Nasir, E. Yang, I. Kakadiaris, F. Flores, S. S. Mao, and M. J. Budoff, "Mortality incidence and the severity of coronary atherosclerosis assessed by computed tomography angiography," *J. Amer. College Cardiol.*, vol. 52, no. 16, pp. 1335–1343, Oct. 2008.

[7] W.-T. Chen, C.-H. Yu, and C.-W. Sun, "Altered near-infrared spectroscopy response to breath-holding in patients with fibromyalgia," *J. Biophoton.*, vol. 12, no. 1, Jan. 2019, Art. no. e201800142.

[8] S. Waxman, S. R. Dixon, P. L'Allier, J. W. Moses, J. L. Petersen, D. Cutlip, J. C. Tardif, R. W. Nesto, J. E. Muller, M. J. Hendricks, S. T. Sum, C. M. Gardner, J. A. Goldstein, G. W. Stone, and M. W. Krucoff, "*In vivo* validation of a catheter-based near-infrared spectroscopy system for detection of lipid core coronary plaques: Initial results of the SPECTACL study," *JACC Cardiovascular Imag.*, vol. 2, no. 7, pp. 858–868, 2009.

[9] R. P. Rao, M. J. Danduran, R. S. Loomba, J. E. Dixon, and G. M. Hoffman, "Near-infrared spectroscopic monitoring during cardiopulmonary exercise testing detects anaerobic threshold," *Pediatric Cardiol.*, vol. 33, no. 5, pp. 791–796, Jun. 2012.

[10] J. P. Scott and G. M. Hoffman, "Near-infrared spectroscopy: Exposing the dark (venous) side of the circulation," *Pediatric Anesthesia*, vol. 24, no. 1, pp. 74–88, Jan. 2014.

[11] K. Albouaini, M. Egred, A. Alahmar, and D. J. Wright, "Cardiopulmonary exercise testing and its application," *Postgraduate Med. J.*, vol. 83, no. 985, pp. 675–682, Nov. 2007.

[12] A. K. F. D. Silva, M. P. D. C. D. R. Barbosa, A. F. B. Bernardo, F. M. Vanderlei, F. L. Pacagnelli, and L. C. M. Vanderlei, "Cardiac risk stratification in cardiac rehabilitation programs: A review of protocols," *Revista Brasileira de Cirurgia Cardiovascular*, vol. 29, no. 2, pp. 255–265, 2014.

[13] J.-R. Kuo, B.-S. Lin, C.-L. Cheng, and C.-C. Chio, "Hypoxic-state estimation of brain cells by using wireless near-infrared spectroscopy," *IEEE J. Biomed. Health Inform.*, vol. 18, no. 1, pp. 167–173, Jan. 2014.

[14] Y.-K. Huang, C.-C. Chang, P.-X. Lin, and B.-S. Lin, "Quantitative evaluation of rehabilitation effect on peripheral circulation of diabetic foot," *IEEE J. Biomed. Health Inform.*, vol. 22, no. 4, pp. 1019–1025, Jul. 2018.

[15] W. G. Zijlstra, A. Buursma, and O. W. van Assendelft, *Visible and Near Infrared Absorption Spectra of Human and Animal Haemoglobin Determination and Application*. Rancho Cordova, CA, USA: VSP, 2000.

[16] D. T. Delpy, M. Cope, P. V. D. Zee, S. Arridge, S. Wray, and J. Wyatt, "Estimation of optical pathlength through tissue from direct time of flight measurement," *Phys. Med. Biol.*, vol. 33, no. 12, pp. 1433–1442, Dec. 1988.

[17] S. Fantini, D. Hueber, M. A. Franceschini, E. Gratton, W. Rosenfeld, P. G. Stubblefield, D. Maulik, and M. R. Stankovic, "Non-invasive optical monitoring of the newborn piglet brain using continuous-wave and frequency-domain spectroscopy," *Phys. Med. Biol.*, vol. 44, no. 6, pp. 1543–1562, 1999.

[18] F. Scholkmann and M. Wolf, "General equation for the differential pathlength factor of the frontal human head depending on wavelength and age," *J. Biomed. Opt.*, vol. 18, no. 10, Oct. 2013, Art. no. 105004.

[19] A. M. Chiarelli, D. Perpetuini, C. Filippini, D. Cardone, and A. Merla, "Differential pathlength factor in continuous wave functional near-infrared spectroscopy: Reducing hemoglobin's cross talk in high-density recordings," *Neurophotonics*, vol. 6, no. 3, 2019, Art. no. 035005.

[20] J.-R. Kuo, M.-H. Chang, C.-C. Wang, C.-C. Chio, J.-J. Wang, and B.-S. Lin, "Wireless near-infrared spectroscopy system for determining brain hemoglobin levels in laboratory animals," *J. Neurosci. Methods*, vol. 214, no. 2, pp. 204–209, Apr. 2013.

[21] P. Pinti, F. Scholkmann, A. Hamilton, P. Burgess, and I. Tachtsidis, "Current status and issues regarding pre-processing of fNIRS neuroimaging data: An investigation of diverse signal filtering methods within a general linear model framework," *Frontiers Hum. Neurosci.*, vol. 12, p. 505, Dec. 2018.

[22] B. Molavi and G. A. Dumont, "Wavelet-based motion artifact removal for functional near-infrared spectroscopy," *Physiological Meas.*, vol. 33, no. 2, pp. 259–270, Feb. 2012.

[23] D. Formenti, D. Perpetuini, P. Iodice, D. Cardone, G. Michielon, R. Scurati, G. Alberti, and A. Merla, "Effects of knee extension with different speeds of movement on muscle and cerebral oxygenation," *PeerJ*, vol. 6, Oct. 2018, Art. no. e5704.

[24] L. Pollonini, "Optical properties and molar hemoglobin concentration of skeletal muscles measured *in vivo* with wearable near infrared spectroscopy," *IEEE Sensors J.*, vol. 18, no. 6, pp. 2326–2334, Mar. 2018.

[25] S. Elanayar V. T. and Y. C. Shin, "Radial basis function neural network for approximation and estimation of nonlinear stochastic dynamic systems," *IEEE Trans. Neural Netw.*, vol. 5, no. 4, pp. 594–603, Jul. 1994.

[26] B.-S. Lin, B.-S. Lin, F.-C. Chong, and F. Lai, "Higher-order-statistics-based radial basis function networks for signal enhancement," *IEEE Trans. Neural Netw.*, vol. 18, no. 3, pp. 823–832, May 2007.

[27] J. C. Bezdek, "Objective function clustering," in *Pattern Recognition With Fuzzy Objective Function Algorithms*. New York, NY, USA: Springer, 1981, pp. 43–93.

[28] L. M. Oldervoll, S. Kaasa, M. J. Hjermstad, J. Å. Lund, and J. H. Loge, "Physical exercise results in the improved subjective well-being of a few or is effective rehabilitation for all cancer patients?" *Eur. J. Cancer*, vol. 40, no. 7, pp. 951–962, May 2004.

[29] M. S. Irwin, M. S. Thorniley, C. J. Dore, and C. J. Green, "Near infra-red spectroscopy: A non-invasive monitor of perfusion and oxygenation within the microcirculation of limbs and flaps," *Brit. J. Plastic Surg.*, vol. 48, no. 1, pp. 14–22, 1995.

[30] K. J. Smith and P. N. Ainslie, "Regulation of cerebral blood flow and metabolism during exercise," *Experim. Physiol.*, vol. 102, no. 11, pp. 1356–1371, Nov. 2017.

[31] A. Koike, H. Itoh, R. Oohara, M. Hoshimoto, A. Tajima, T. Aizawa, and L. T. Fu, "Cerebral oxygenation during exercise in cardiac patients," *Chest*, vol. 125, no. 1, pp. 182–190, Jan. 2004.

WILLY CHOU received the B.S. degree from the Medicine Department, National Taiwan University, Taiwan, in 1989, and the M.S. degree from the Department of Human Resource Management, Hospital Management Team, National Sun Yat-sen University, Taiwan, in 2003. He is currently a Professor of Ministry of Education and the Department of Rehabilitation, Chi Mei Medical Center, Taiwan. His research interests include exercise physiology, cardiopulmonary rehabilitation, and human resource management.

PEI-JUNG WU received the B.S. degree in electrical engineering from the National Changhua University of Education, Taiwan, in 2008, the M.S. degree in electronic engineering from the National Yunlin University of Science and Technology, Taiwan, in 2012, and the Ph.D. degree in imaging and biomedical photonics from National Chiao Tung University (NCTU), Taiwan, in 2018. She is currently an Assistant Professor with the College of Information and Distribution Science, National Taichung University of Science and Technology, Taiwan. Her research interests include 3-D displays, biomedical signal processing, and human factors.

CHIH-CHIEH FANG received the M.S. degree from the Institute of Photonic System, National Chiao Tung University (NCTU), Taiwan, in 2019. His research interests include biomedical circuits and systems, biomedical signal processing, and biosensor.

YUN-SHAN YEN received the Medical degree from National Cheng Kung University (NCKU), Taiwan, in 2013. She is currently an Attending Physician with the Division of Rehabilitation Medicine, Chia-Yi Christian Hospital. Her research interest includes cardiopulmonary rehabilitation.

BOR-SHYH LIN (Senior Member, IEEE) received the B.S. degree from National Chiao Tung University (NCTU), Taiwan, in 1997, and the M.S. degree in electrical engineering and the Ph.D. degree in electrical engineering from National Taiwan University (NTU), Taiwan, in 1999 and 2006, respectively. He is currently a Professor with the Institute of Imaging and Biomedical Photonics, NCTU. His research interests include biomedical circuits and systems, biomedical signal processing, and biosensor.